Hot electron cooling in graphite: Supercollision versus hot phonon decay

A. Stange,[1,*] C. Sohrt,[1] L. X. Yang,[1,2] G. Rohde,[1] K. Janssen,[1] P. Hein,[1] L.-P. Oloff,[1] K. Hanff,[1] K. Rossnagel,[1] and M. Bauer[1]
[1]*Institut für Experimentelle und Angewandte Physik, Christian-Albrechts-Universität zu Kiel, D-24098 Kiel, Germany*
[2]*Physics Department, Tsinghua University, Beijing 100089, People's Republic of China*
(Received 13 July 2015; revised manuscript received 16 September 2015; published 20 November 2015)

Disorder-assisted electron-phonon scattering processes (supercollision processes) have been reported to dominate the cooling of hot carriers in graphene. Here, we determine to what extent this type of relaxation mechanism governs the hot carrier dynamics in the parent compound graphite. Electron temperature transients derived from time- and angle-resolved extreme ultraviolet photoemission spectra are analyzed based on a three-temperature model which considers electron gas, optical phonons, and acoustic phonons as coupled subsystems. In the probed fluence regime of 0.035–1.4 mJ/cm^2, we find no indications for supercollision processes being involved in the cooling of the hot carriers. The data are, by contrast, compatible with a hot phonon assisted mechanism involving anharmonic coupling between optical phonons and acoustic phonons, a process which has previously been suggested for graphite. We attribute the striking difference to the reported findings for (substrate-supported) graphene to the low defect density of highly ordered pyrolitic graphite.

DOI: 10.1103/PhysRevB.92.184303 PACS number(s): 79.60.−i, 81.05.ue, 78.47.J−, 63.20.kd

I. INTRODUCTION

Next to its unique band structure, the exceptional electronic and optical properties of graphene stem in large part from an intrinsically weak coupling of the charge carriers to the phonons going along with long electron-hole relaxation times and small electron-lattice cooling rates [1–4]. In recent years, this peculiarity has stimulated numerous studies on the fundamental aspects of electron-lattice interaction in graphene and its parent compound graphite [5–13]. The common view on this problem, as addressed in ultrafast pump-probe spectroscopy experiments, is illustrated in Fig. 1. After the heating up of the electron gas by absorption of an intense optical pump pulse, a rapid decrease in the electron temperature T_e within a few hundred femtoseconds is observed which is attributed to the thermalization with a reservoir of strongly coupled optical phonons (SCOPs) [6,12,14]. Subsequent heating of the acoustic phonon (AP) bath is typically observed on a time scale of several picoseconds; the assignment of this process to a specific coupling channel is, however, less obvious. From a theory standpoint, momentum mismatch considerably suppresses in the first instance the efficiency of the direct coupling channel between electrons and APs yielding cooling times exceeding 300 ps [3,12], incompatible with the experimental observations. Different heat-transfer pathways have been proposed instead. In the case of graphite, experimental results implied that the heat transfer occurs via a hot phonon assisted (HP) process involving the SCOPs as an intermediate reservoir which decay through anharmonic coupling to lower-energy APs [14,15]. In addition, recent studies on graphene emphasized the role of disorder which can act as a momentum source substantially promoting a direct coupling between electrons and APs via so-called supercollision (SC) processes [16–18]. This model succeeded in describing experimental data up to peak electron temperatures of several thousand Kelvin [19,20], although it was primarily developed to account for the findings at low temperatures at which efficient coupling to the high-energy optical phonons is considerably suppressed. An interpretation in favor of the SC model was further substantiated by a comparative study showing that the HP scenario quantitatively fails to describe the dynamics of hot electron cooling in graphene [21].

In light of the intimate relation between graphene and graphite, the reports on fundamentally different phononic pathways for energy dissipation are astonishing. However, an evaluation of graphite data on the basis of a SC scenario has not been conducted so far, although it is necessary for the conclusive examination of such a striking difference between these two materials.

Based on the analysis of time- and angle-resolved photoemission (trARPES) data, we show in this paper that for highly ordered pyrolitic graphite (HOPG) and at excitation fluences $F \geqslant 35\ \mu$J/cm^2, SC processes are, if at all, only of minor relevance for the heat exchange between the laser-excited electron gas and the lattice. In contrast, the experimental data are exceptionally well reproduced under

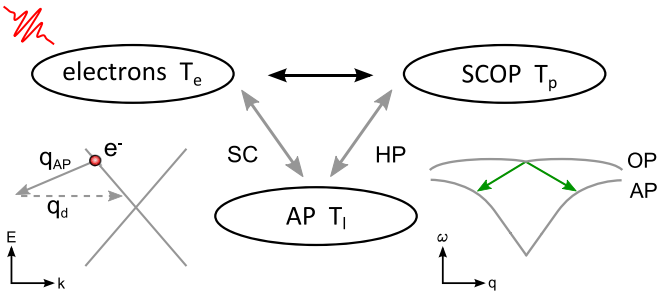

FIG. 1. (Color online) Schematic illustration of potential electron-phonon coupling channels for hot carrier cooling in graphite and graphene. Supercollision (SC) scattering processes (left) allow overcoming the intrinsic momentum imbalance q_d in the direct coupling between electrons and acoustic phonons (AP) with q_{AP} being the AP momentum. In the hot phonon (HP) scenario (right), the coupling to the lattice involves optical phonons (OP) which decay into lower-energy APs through anharmonic coupling (green arrows).

*stange@physik.uni-kiel.de

the assumption of a HP scenario. We suggest that the observation of the dominant electron-phonon coupling channel in HOPG being different from the findings for graphene results from the presence of extrinsic impurities typically reported for substrate-supported graphene [22,23]. Our experimental results on HOPG may therefore provide a benchmark for the suppression of electron-phonon interaction achievable in low-defect suspended graphene samples.

II. EXPERIMENT

In our study, we investigated bulk samples of HOPG (Goodfellow Ltd.). Graphite samples were cleaved under high vacuum conditions (1×10^{-7} mbar) right before the photoemission measurements which were conducted at a base pressure of 4×10^{-10} mbar. TrARPES experiments were performed in a pump-probe configuration using 30-fs near-infrared (NIR, 1.6 eV) pump pulses delivered by a 8-kHz Ti:sapphire multipass amplifier as well as sub-10-fs extreme-ultraviolet (XUV, 22.1 eV) probe pulses from a high-harmonic generation (HHG) source driven by the second harmonic of the laser output [25,26]. Photoelectron spectra were recorded with a hemispherical analyzer at an energy resolution of 240 meV limited by the spectral width of the harmonics (<170 meV) and the used settings of the analyzer. Incident pump fluences F ranged from 0.035 to 1.4 mJ/cm^2. NIR and XUV pulses were focused almost collinearly onto the sample surface and cross correlation measurements at the sample position yielded 32 fs FWHM. All data were measured at an equilibrium sample temperature of 100 K.

III. RESULTS AND DISCUSSION

Figure 2(a) shows trARPES data of graphite in the vicinity of the H point and around E_F with the pump-probe time delay set to $\Delta t = -500$ fs, i.e., prior to the excitation by the NIR pulse. Location and extent of the sampled region within the $\vec{k}$ space of graphite are marked by the trapezoidally shaped area in Fig. 2(b). The downward-dispersing π band of HOPG is well resolved and no indications for an occupation of the upward-dispersing π^* band are observed, as expected for an undoped sample at thermal equilibrium. Figures 2(c)–2(e) show trARPES data recorded at a pump fluence of 0.56 mJ/cm^2 for time delays $\Delta t > 0$, i.e., after excitation by the NIR pulse. Absorption of the pump pulse results in the transient population of the π^* band above E_F which decays on a time scale of several picoseconds. Difference intensity maps unveil also the corresponding transient depopulation of the occupied π band [Figs. 2(f)–2(h)]. Qualitatively similar experimental data were reported recently in trARPES studies on graphene [20,27].

A. Data analysis

A quantitative analysis of the nonequilibrium response of the photoexcited graphite was performed by comparing momentum-integrated energy distribution curves (EDCs) derived from the trARPES snapshots with Fermi-Dirac (FD) distribution functions $f(E) = \{\exp[(E-\mu)/k_B T_e] + 1\}^{-1}$, with μ being the chemical potential. For such a comparison it is,

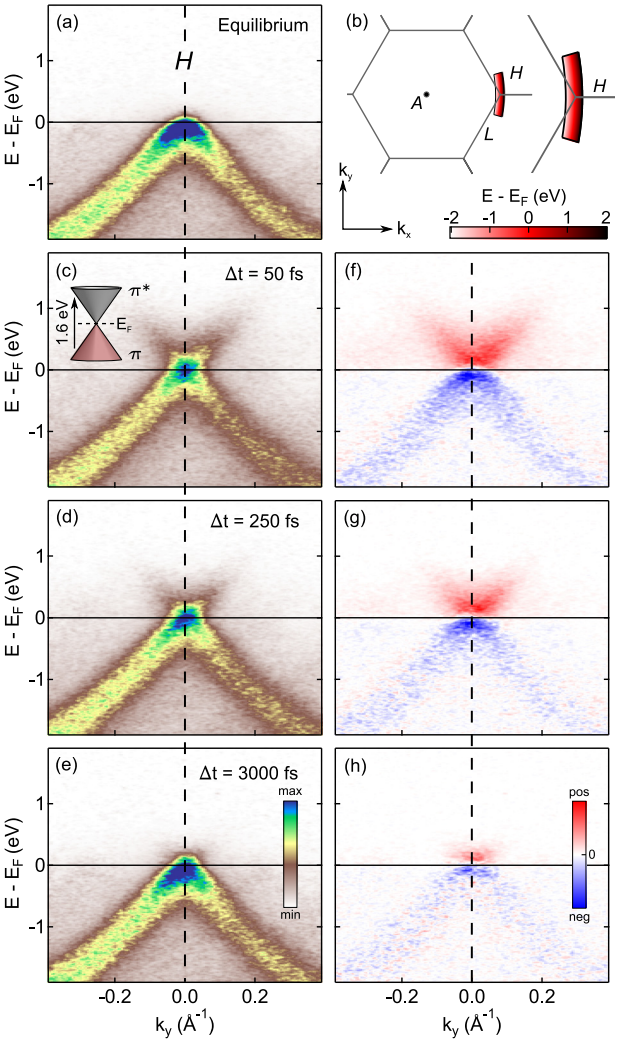

FIG. 2. (Color online) Time-resolved ARPES data of HOPG for $F = 0.56$ mJ/cm^2 near the H point. (a) ARPES band map recorded with HHG light ($h\nu = 22.1$ eV) at 100 K in equilibrium, i.e., 500 fs before excitation. (b) Brillouin zone of graphite with the energy-momentum area mapped in the experiment indicated. (c)–(e) ARPES snapshots recorded at different time delays Δt after excitation. The inset in (c) illustrates the photoexcitation from the π to the π^* band at $h\nu = 1.6$ eV. A movie generated from a complete set of trARPES data is part of Ref. [24]. (f)–(h) Difference intensity maps derived from (c)–(e) in reference to the equilibrium data.

however, indispensable to first correct the experimental EDCs for density of states [28], interference [29], and photoemission matrix-element effects. The latter are of particular relevance in the case of graphite and graphene due to the different symmetries of the π and π^* bands [30–32]. Details on our correction procedure are given in Ref. [24].

The corrected EDCs for different time delays ($F = 1.4$ mJ/cm^2) are compared in Fig. 3(a) with the raw data shown for reference in the inset. The graph also includes FD distribution functions convoluted with a Gaussian representing the experimental energy resolution fitted to the corrected EDCs with T_e and μ used as fitting parameters. Notably and contrary to the raw data, for most time delays,

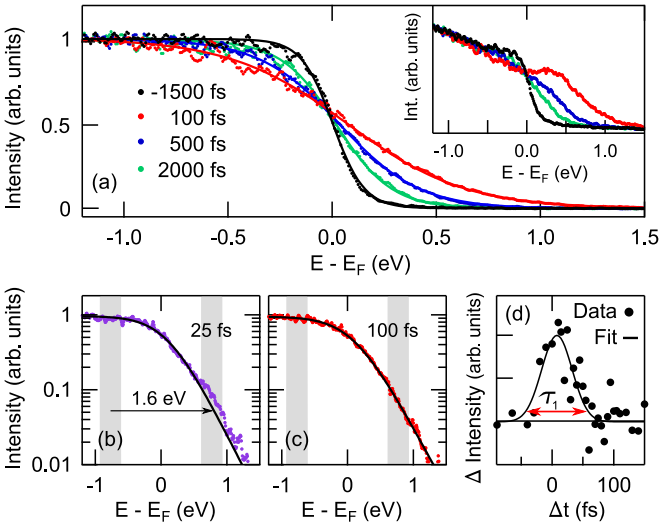

FIG. 3. (Color online) EDCs around E_F derived from trARPES data at $F = 1.4$ mJ/cm^2. (a) EDCs for different Δt in comparison to fits which assume a thermalized Fermi-Dirac distribution (solid lines). The EDCs were derived from trARPES data integrated along k_y (cf. Fig. 2) and corrected as described in Ref. [24]. The corresponding raw data are shown in the inset. Photoemission intensity was integrated over a momentum window of 0.8 Å^{-1}. (b), (c) Corrected EDCs for $\Delta t = 25$ and 100 fs (logarithmic scale) in comparison to the fit to illustrate the deviation from a thermalized electron distribution shortly after photoexcitation. (d) Nonthermal component of the EDCs as a function of Δt: τ_1 was estimated from the full width at 10% of the maximum of a Gaussian fit to the transients.

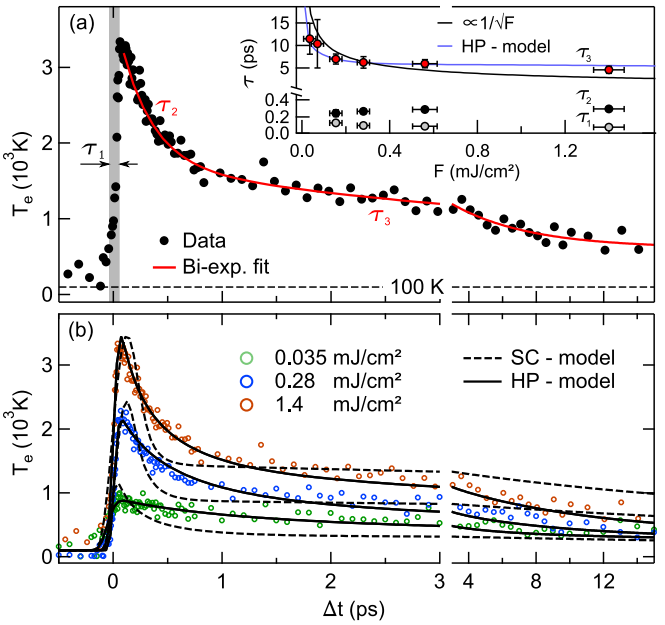

FIG. 4. (Color online) (a) T_e transients for $F = 1.4$ mJ/cm^2 derived from FD fits to the EDCs. The red solid line is a biexponential fit to the data. The inset summarizes the characteristic time scales of electron cooling as a function of excitation fluence F derived from the experimental data. τ_2 and τ_3 are the results of the biexponential fits to the T_e transients. The black line indicates a $F^{-1/2}$ scaling as expected for τ_3 within the SC model [21]. The blue line is the corresponding result within the HP model. (b) Experimental T_e transients for different fluences in comparison to 3TM fits (dashed line: SC model; solid line: HP model).

the FD fits reproduce the corrected EDCs extremely well. This particularly applies also to the EDC prior to excitation recorded at $\Delta t = -1500$ fs. Clear deviations can only be observed for EDCs recorded shortly after photoexcitation [$\Delta t \lesssim 100$ fs, cf. Figs. 3(b) and 3(c)]. On these short time scales we observe an increase in the electron and hole population at energies $E - E_F \simeq \pm 0.8$ eV, respectively. We associate these spectral signatures with the nonthermal and short-lived nascent electron distribution that is expected for the absorption of a pump pulse at $h\nu = 1.6$ eV.

B. Characteristic time scales and chemical potential

Figure 3(d) depicts the energy-integrated difference between corrected EDCs and fitted FD distributions as a function of time for $F = 1.4$ mJ/cm^2. The data indicate that a thermalized carrier distribution is established within $\tau_1 \lesssim 100$ fs consistent with the presence of highly efficient scattering processes driving the internal thermalization of the electron gas. Clear indications for a fluence dependence of the internal thermalization time τ_1 are not observed [inset in Fig. 4(a)]. Similar time scales for τ_1 were reported in other studies on graphite and graphene before [33–35] and were interpreted in terms of Coulomb-dominated scattering among the excited carriers [36].

In a next step, we generate electron temperature transients from the FD fits. Results for $F = 1.4$ mJ/cm^2 are shown in Fig. 4(a). In agreement with results of previous studies [33,37], the cooling of the electron gas after the initial excitation follows a biexponential behavior. The fast component τ_2 is caused by the efficient energy transfer from highly excited electrons to SCOP modes at Γ and K [5,38]. The fits yield values of $\tau_2 \approx 250$ fs which agree very well with reference data reported in Refs. [6,33,37]. The slow component τ_3 is generally associated with the heat up of the acoustic phonon bath [6,39] and clearly decreases as the excitation fluence increases [inset of Fig. 4(a)]. The observed time scales of several ps for τ_3 agree once again very well with the results from other studies [6,14,15,39].

We briefly comment on the results for the second fit parameter, the chemical potential μ. Figure 5 summarizes chemical potential data from different fluence runs as a

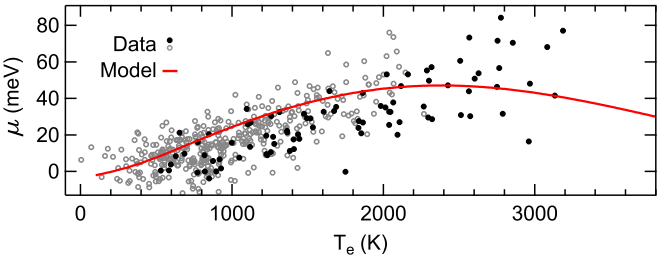

FIG. 5. (Color online) Temperature dependence of the chemical potential μ derived from the FD fits. The solid line shows the calculated T_e dependence under consideration of a purely metallic response of the electronic system.

function of T_e. The observed correlation between μ and T_e is consistent with a metallic behavior of the electronic system, as verified by a parameter-free calculation of μ under consideration of realistic data for the electron density of states [28] (solid line in Fig. 5).

Notably, other works on the transient response of μ in graphite and graphene have reported different results. Based on transient absorption data, Breusing *et al.* [33] reported for graphite on a separation of electron and hole chemical potential by several 100 meV for at least 1 ps, indicative for semiconductor-type behavior. A transient separation of the electron and hole chemical potential was also observed for graphene in a trARPES study, restricted, however, to the first 130 fs after photoexcitation [27], i.e., within the time regime where the trARPES data of this study clearly imply a nonthermalized carrier distribution.

C. Supercollision and hot phonon model

We now come back to the temporal evolution of T_e which reflects the peculiarities of the possible coupling pathways between the electron and phonon systems, as schematically illustrated in Fig. 1.

In order to elucidate the relevance of the different processes, we performed fits to the measured electron temperature transients on the basis of a three-temperature model (3TM) [40] under consideration of SC and HP scenarios, respectively.

This model considers electron gas, optical phonons, and acoustic phonons as three thermalized subsystems and describes the temporal evolution of the corresponding temperatures T_e, T_p, and T_l by a set of coupled differential equations. In a general form, this set of equations can be written as

$$\begin{aligned} C_e\dot{T}_e &= S(t) - \Gamma_{ep} - \Gamma_{el}, \\ C_p\dot{T}_p &= \Gamma_{ep} - \Gamma_{pl}, \\ C_l\dot{T}_l &= \Gamma_{el} + \Gamma_{pl}, \end{aligned}$$

where $S(t)$ accounts for the initial heat up of the electron gas by absorption of the laser pulse, C_e, C_p, and C_l are the heat capacities of the electron gas, optical phonons, and acoustic phonons, respectively, and Γ_{ep}, Γ_{el}, and Γ_{pl} are the heat-transfer rates between the coupled reservoirs.

The heat transfer between electron gas and optical phonons is driven by SCOP-mediated intraband and interband scattering processes and therefore depends on the thermal population of optical phonons and the available phase space for the electrons. In an integral form Γ_{ep} can be approximated by the following expression [9,41,42]:

$$\begin{aligned} \Gamma_{ep} =& \beta[1 + n(T_p)] \\ &\times \int D(E)D(E - \hbar\omega_0)f(E)[1 - f(E - \hbar\omega_0)]dE \\ &- \beta n(T_p) \int D(E)D(E + \hbar\omega_0)f(E) \\ &\times [1 - f(E + \hbar\omega_0)]dE. \end{aligned} \quad (1)$$

Here, the optical phonon system is described in an Einstein model with ω_0 being the Einstein frequency yielding a phonon distribution $n(T_p) = [\exp(\hbar\omega_0/k_B T_p) - 1]^{-1}$. The parameter β accounts for the coupling strength between electrons and optical phonons.

For the description of the experimental data within a HP coupling scenario, we disregarded Γ_{el}, i.e., we completely neglected direct coupling between electrons and acoustic phonons. To account for the heat transfer between optical phonons and acoustic phonons, the following common expression for Γ_{pl} was used [9,40]:

$$\Gamma_{pl} = \gamma C_p(T_p - T_l),$$

where γ denotes the energy decay rate of the hot SCOP system.

In the SC approximation, we neglected coupling between optical and acoustic phonons, i.e., $\Gamma_{pl} = 0$. Under consideration of SC processes, one finds furthermore [16]

$$\Gamma_{el} = A\left(T_e^3 - T_l^3\right),$$

with the rate coefficient A given by

$$A = 9.62\frac{g^2 D^2(\mu)k_B^3}{\hbar k_F l}. \quad (2)$$

Here, k_F is the Fermi vector, g is the electron-phonon coupling constant, $D(\mu)$ is the density of states at the chemical potential, and l is the electron mean-free path due to disorder by short-range scatterers. According to Graham *et al.* [19,21], one can alternatively account for the temperature dependence of A by the following expression:

$$A = k\frac{C_e}{T_e}$$

with k being a scaling constant independent of temperature.

In order for the fits to provide physical meaningful results, a careful investigation on the relevant parameters must be undertaken, particularly with respect to their potential temperature dependence. C_e was approximated by an expansion up to third order in T_e given in [43] combining calculations based on a three-dimensional band model and experimental data for graphite measured at low temperatures. To account for the temperature dependence of C_p, we referred to a study by Lui *et al.* [42] who derived an analytic expression based on experimental data of a time-resolved Raman study of graphite [14]. C_l was calculated from the difference between the total heat capacity of the lattice, C_t and C_p. A closed expression for C_t of graphite based on different sets of experimental data in a wide temperature range can be found in [43]. Finally, the heat-transfer rate Γ_{ep} was calculated according to Eq. (1) with the Einstein frequency $\hbar\omega_0 = 200$ meV and with $D(E)$ taken from [28].

In the SC scenario, we left k, β, and S_0 as the temperature-independent fitting parameters with S_0 being the amplitude of the excitation. In the HP scenario, γ, β, and S_0 were kept free. For consistency, we determined in a first step k, β, and γ by a fit to the data recorded at $F = 1.4$ mJ/cm^2. These values were used as a fixed input for all other data sets which were then fitted with S_0 left as the only free parameter. Note that due to saturation effects, a linear dependence of S_0 on the incident fluence can in general not be presumed [35,44].

Experimental temperature transients and the results of the 3TM fits are compared for different excitation fluences in Fig. 4(b): For all fluences, the SC model clearly fails to describe the experimental data. In fact, even the data set

which was fitted with all three fitting parameters left free ($F = 1.4$ mJ/cm^2) cannot satisfactorily be reproduced by the SC model. In contrast, independent of fluence the HP model shows a very good agreement with the experimental data. Notably, also the smallest fluence data are very well reproduced by the fit, even though the maximum electron temperature of 900 K, corresponding to a thermal energy of 78 meV, is well below the optical phonon energy of about 200 meV. We speculate that even at this temperature, the FD-distributed electron gas provides enough hot electrons and holes for a sufficiently efficient energy transfer into the optical phonon system. Such an interpretation conforms to recent results of a mid-infrared study of graphene [11]. For the electron-phonon coupling parameter β, the fit within the HP model yields a value of $\beta = 2.1$ eV^2 cm^2 s^{-1} in reasonable agreement with a reference value of $\beta = 5$ eV^2 cm^2 s^{-1} reported for graphene [42]. For the energy decay rate of the hot SCOP system, the fit yields a value of $\gamma = 110$ GHz, in very good agreement with an experimental value of 100 GHz reported in Ref. [15]. The 3TM fitting results are additionally supported by a comparison of the experimental data on the fluence dependence of τ_3 with predictions from the SC model and the HP model, respectively, shown in the inset of Fig. 4(a). In a cooling scenario dominated by SC processes, theory predicts a scaling of $\tau_3 \propto F^{-1/2}$ [19]. For the HP case, we derived the expected fluence dependence τ_3 from biexponential fits to T_e transients simulated within the 3TM model. Once again, the comparison between experiment and model is clearly in favor of the HP scenario.

The most apparent signature of the SC scenario conflicting with the experimental data is the rapid transition from the fast to the slow component in the electron cooling process. It arises from the sudden closure of the optical phonon channel as soon as a thermal equilibrium with the electron gas is established. The HP model describes the smooth transition observed in the experiment much better. Here, the acoustic phonon bath acts as a permanent heat drain for the optical phonons. As T_e and T_p converge, the heat transfer between the two systems slows down. The optical phonon channel is, however, never closed completely.

D. Comparison with graphene

Recently, two independent studies reported on SC cooling being the dominating process in graphene coupling electron gas and acoustic phonon bath up to electron temperatures of 3000 K [17,19]. This interpretation was further supported by a 3TM analysis of trARPES data of graphene [20]. The results seemingly disagree with our findings for graphite even though the characteristic energy and momentum scales offered by optical and acoustic phonon bath are basically the same for both materials. However, as can be seen from Eq. (2), the SC mechanism critically depends on the chemical potential μ and the electron mean-free path l (as limited by disorder), two parameters which may vary significantly between the different samples. Indeed, at least part of the studies on SC cooling in graphene were reported on doped samples [19,20], yielding different values of μ in comparison to the undoped graphite sample used in this study. Explicit evidence for the relevance of l in the SC process was recently given in a study on laser-treated graphene [18]. Furthermore, low-temperature conductivity measurements of pristine suspended graphene implied the relevance of charged impurity scattering limiting l to values of $\approx$150 nm (this value increases into the μm regime after thermal treatment) [2]. Due to the presence of substrate disorder, even smaller values of l are observed in the case of substrate-supported graphene, the type of sample used in the studies on SC cooling. Here, typical impurity densities of $\sim 10^{12}$ cm^{-2} are to be expected [45], in good agreement with the quantitative interpretations of graphene data in terms of the supercollision model [17–20]. In contrast, conductivity studies on HOPG yield l values in the μm range [46], a result which is also supported by Raman studies [47]. This striking difference particularly in comparison to substrate-supported graphene samples may explain why SC cooling is considerably suppressed in pristine HOPG.

IV. CONCLUSION

In conclusion, our trARPES study clearly confirms earlier work on graphite which proposed hot phonon mediated relaxation processes being a relevant channel which couples electron gas and lattice [14,15]. More importantly, the data show that supercollision processes are not of relevance for hot electron cooling in HOPG at least in the addressed fluence regime, in striking contrast to quite a number of recent reports of graphene. Substantial differences in the extrinsic impurity density in graphene due to interaction with a supporting substrate is a likely origin of this remarkable difference. The results emphasize again the relevance of disorder as a distinct parameter determining physical properties of graphene.

ACKNOWLEDGMENTS

This work was supported by the German Science Foundation (DFG) through Project No. BA 2177/9-1. L.X.Y. is grateful to the Alexander von Humboldt foundation for support.

[1] E. H. Hwang, S. Adam, and S. Das Sarma, Carrier Transport in Two-Dimensional Graphene Layers, Phys. Rev. Lett. **98**, 186806 (2007).

[2] K. I. Bolotin, K. J. Sikes, J. Hone, H. L. Stormer, and P. Kim, Temperature-Dependent Transport in Suspended Graphene, Phys. Rev. Lett. **101**, 096802 (2008).

[3] R. Bistritzer and A. H. MacDonald, Electronic Cooling in Graphene, Phys. Rev. Lett. **102**, 206410 (2009).

[4] A. C. Betz, F. Vialla, D. Brunel, C. Voisin, M. Picher, A. Cavanna, A. Madouri, G. Fève, J.-M. Berroir, B. Plaçais, and E. Pallecchi, Hot Electron Cooling by Acoustic Phonons in Graphene, Phys. Rev. Lett. **109**, 056805 (2012).

[5] S. Piscanec, M. Lazzeri, F. Mauri, A. C. Ferrari, and J. Robertson, Kohn Anomalies and Electron-Phonon Interactions in Graphite, Phys. Rev. Lett. **93**, 185503 (2004).

[6] T. Kampfrath, L. Perfetti, F. Schapper, C. Frischkorn, and M. Wolf, Strongly Coupled Optical Phonons in the Ultrafast Dynamics of the Electronic Energy and Current Relaxation in Graphite, Phys. Rev. Lett. **95**, 187403 (2005).

[7] A. Bostwick, T. Ohta, T. Seyller, K. Horn, and E. Rotenberg, Quasiparticle dynamics in graphene, Nat. Phys. **3**, 36 (2007).

[8] C. S. Leem, C. Kim, S. R. Park, M.-K. Kim, H. J. Choi, C. Kim, B. J. Kim, S. Johnston, T. Devereaux, T. Ohta, A. Bostwick, and E. Rotenberg, High-resolution angle-resolved photoemission studies of quasiparticle dynamics in graphite, Phys. Rev. B **79**, 125438 (2009).

[9] H. Wang, J. H. Strait, P. A. George, S. Shivaraman, V. B. Shields, M. Chandrashekhar, J. Hwang, F. Rana, M. G. Spencer, C. S. Ruiz-Vargas, and J. Park, Ultrafast relaxation dynamics of hot optical phonons in graphene, Appl. Phys. Lett. **96**, 081917 (2010).

[10] J. K. Viljas and T. T. Heikkilä, Electron-phonon heat transfer in monolayer and bilayer graphene, Phys. Rev. B **81**, 245404 (2010).

[11] S. Winnerl, M. Orlita, P. Plochocka, P. Kossacki, M. Potemski, T. Winzer, E. Malic, A. Knorr, M. Sprinkle, C. Berger, W. A. de Heer, H. Schneider, and M. Helm, Carrier Relaxation in Epitaxial Graphene Photoexcited Near the Dirac Point, Phys. Rev. Lett. **107**, 237401 (2011).

[12] E. Malic, T. Winzer, E. Bobkin, and A. Knorr, Microscopic theory of absorption and ultrafast many-particle kinetics in graphene, Phys. Rev. B **84**, 205406 (2011).

[13] B. Gao, G. Hartland, T. Fang, M. Kelly, D. Jena, H. G. Xing, and L. Huang, Studies of intrinsic hot phonon dynamics in suspended graphene by transient absorption microscopy, Nano Lett. **11**, 3184 (2011).

[14] H. Yan, D. Song, K. F. Mak, I. Chatzakis, J. Maultzsch, and T. F. Heinz, Time-resolved Raman spectroscopy of optical phonons in graphite: Phonon anharmonic coupling and anomalous stiffening, Phys. Rev. B **80**, 121403(R) (2009).

[15] M. Scheuch, T. Kampfrath, M. Wolf, K. von Volkmann, C. Frischkorn, and L. Perfetti, Temperature dependence of ultrafast phonon dynamics in graphite, Appl. Phys. Lett. **99**, 211908 (2011).

[16] J. C. W. Song, M. Y. Reizer, and L. S. Levitov, Disorder-Assisted Electron-Phonon Scattering and Cooling Pathways in Graphene, Phys. Rev. Lett. **109**, 106602 (2012).

[17] A. C. Betz, S. H. Jhang, E. Pallecchi, R. Ferreira, G. Fève, J.-M. Berroir, and B. Plaçais, Supercollision cooling in undoped graphene, Nat. Phys. **9**, 109 (2012).

[18] T. V. Alencar, M. G. Silva, L. M. Malard, and A. M. de Paula, Defect-induced supercollision cooling of photoexcited carriers in graphene, Nano Lett. **14**, 5621 (2014).

[19] M. W. Graham, S.-F. Shi, D. C. Ralph, J. Park, and P. L. McEuen, Photocurrent measurements of supercollision cooling in graphene, Nat. Phys. **9**, 103 (2013).

[20] J. C. Johannsen, S. Ulstrup, F. Cilento, A. Crepaldi, M. Zacchigna, C. Cacho, I. C. Edmond Turcu, E. Springate, F. Fromm, C. Raidel, T. Seyller, F. Parmigiani, M. Grioni, and P. Hofmann, Direct View of Hot Carrier Dynamics in Graphene, Phys. Rev. Lett. **111**, 027403 (2013).

[21] M. W. Graham, S.-F. Shi, Z. Wang, D. C. Ralph, J. Park, and P. L. McEuen, Transient absorption and photocurrent microscopy show that hot electron supercollisions describe the rate-limiting relaxation step in graphene, Nano Lett. **13**, 5497 (2013).

[22] Y. Kopelevich and P. Esquinazi, Graphene physics in graphite, Adv. Mater. **19**, 4559 (2007).

[23] C. R. Dean, A. F. Young, I. Meric, C. Lee, L. Wang, S. Sorgenfrei, K. Watanabe, T. Taniguchi, P. Kim, K. L. Shepard, and J. Hone, Boron nitride substrates for high-quality graphene electronics, Nat. Nanotechnol. **5**, 722 (2010).

[24] See Supplemental Material at http://link.aps.org/supplemental/10.1103/PhysRevB.92.184303 for a detailed description of the correction of the EDCs as well as for a movie of the trARPES data.

[25] C. Sohrt, A. Stange, M. Bauer, and K. Rossnagel, How fast can a Peierls-Mott insulator be melted? Faraday Discuss. **171**, 243 (2014).

[26] S. Eich, A. Stange, A. Carr, J. Urbancic, T. Popmintchev, M. Wiesenmayer, K. Jansen, A. Ruffing, S. Jakobs, T. Rohwer, S. Hellmann, C. Chen, P. Matyba, L. Kipp, K. Rossnagel, M. Bauer, M. Murnane, H. Kapteyn, S. Mathias, and M. Aeschlimann, Time- and angle-resolved photoemission spectroscopy with optimized high-harmonic pulses using frequency-doubled Ti:Sapphire lasers, J. Electron Spectrosc. Relat. Phenom. **195**, 231 (2014).

[27] I. Gierz, J. C. Petersen, M. Mitrano, C. Cacho, I. C. E. Turcu, E. Springate, A. Stöhr, A. Köhler, U. Starke, and A. Cavalleri, Snapshots of non-equilibrium Dirac carrier distributions in graphene, Nat. Mater. **12**, 1119 (2013).

[28] N. Ooi, A. Rairkar, and J. B. Adams, Density functional study of graphite bulk and surface properties, Carbon **44**, 231 (2006).

[29] E. L. Shirley, L. J. Terminello, A. Santoni, and F. J. Himpsel, Brillouin-zone-selection effects in graphite photoelectron angular distributions, Phys. Rev. B **51**, 13614 (1995).

[30] A. Grüneis, C. Attaccalite, A. Rubio, S. L. Molodtsov, D. V. Vyalikh, J. Fink, R. Follath, and T. Pichler, Preparation and electronic properties of potassium doped graphite single crystals, Phys. Status Solidi B **245**, 2072 (2008).

[31] D. Haberer, L. Petaccia, A. V. Fedorov, C. S. Praveen, S. Fabris, S. Piccinin, O. Vilkov, D. V. Vyalikh, A. Preobrajenski, N. I. Verbitskiy, H. Shiozawa, J. Fink, M. Knupfer, B. Büchner, and A. Grüneis, Anisotropic Eliashberg function and electron-phonon coupling in doped graphene, Phys. Rev. B **88**, 081401(R) (2013).

[32] A. V. Fedorov, N. I. Verbitskiy, D. Haberer, C. Struzzi, L. Petaccia, D. Usachov, O. Y. Vilkov, D. V. Vyalikh, J. Fink, M. Knupfer, B. Büchner, and A. Grüneis, Observation of a universal donor-dependent vibrational mode in graphene, Nat. Commun. **5**, 3257 (2014).

[33] M. Breusing, C. Ropers, and T. Elsaesser, Ultrafast Carrier Dynamics in Graphite, Phys. Rev. Lett. **102**, 086809 (2009).

[34] D. Brida, A. Tomadin, C. Manzoni, Y. J. Kim, A. Lombardo, S. Milana, R. R. Nair, K. S. Novoselov, A. C. Ferrari, G. Cerullo, and M. Polini, Ultrafast collinear scattering and carrier multiplication in graphene, Nat. Commun. **4**, 1987 (2013).

[35] S. Winnerl, F. Göttfert, M. Mittendorff, H. Schneider, M. Helm, T. Winzer, E. Malic, A. Knorr, M. Orlita, M. Potemski, M. Sprinkle, C. Berger, and W. A. de Heer, Time-resolved spectroscopy on epitaxial graphene in the infrared spectral range: relaxation dynamics and saturation behavior, J. Phys.: Condens. Matter **25**, 054202 (2013).

[36] T. Winzer and E. Malic, The impact of pump fluence on carrier relaxation dynamics in optically excited graphene, J. Phys.: Condens. Matter **25**, 054201 (2013).

[37] G. Moos, C. Gahl, R. Fasel, M. Wolf, and T. Hertel, Anisotropy of Quasiparticle Lifetimes and the Role of Disorder in Graphite from Ultrafast Time-Resolved Photoemission Spectroscopy, Phys. Rev. Lett. **87**, 267402 (2001).

[38] J. Maultzsch, S. Reich, C. Thomsen, H. Requardt, and P. Ordejón, Phonon Dispersion in Graphite, Phys. Rev. Lett. **92**, 075501 (2004).

[39] R. P. Chatelain, V. R. Morrison, B. L. M. Klarenaar, and B. J. Siwick, Coherent and Incoherent Electron-Phonon Coupling in Graphite Observed with Radio-Frequency Compressed Ultrafast Electron Diffraction, Phys. Rev. Lett. **113**, 235502 (2014).

[40] L. Perfetti, P. A. Loukakos, M. Lisowski, U. Bovensiepen, H. Eisaki, and M. Wolf, Ultrafast Electron Relaxation in Superconducting $Bi_2Sr_2CaCu_2O_{8+\delta}$ by Time-Resolved Photoelectron Spectroscopy, Phys. Rev. Lett. **99**, 197001 (2007).

[41] F. Rana, P. A. George, J. H. Strait, J. Dawlaty, S. Shivaraman, M. Chandrashekhar, and M. G. Spencer, Carrier recombination and generation rates for intravalley and intervalley phonon scattering in graphene, Phys. Rev. B **79**, 115447 (2009).

[42] C. H. Lui, K. F. Mak, J. Shan, and T. F. Heinz, Ultrafast Photoluminescence from Graphene, Phys. Rev. Lett. **105**, 127404 (2010).

[43] T. Nihira and T. Iwata, Temperature dependence of lattice vibrations and analysis of the specific heat of graphite, Phys. Rev. B **68**, 134305 (2003).

[44] K. Seibert, G. C. Cho, W. Kütt, H. Kurz, D. H. Reitze, J. I. Dadap, H. Ahn, M. C. Downer, and A. M. Malvezzi, Femtosecond carrier dynamics in graphite, Phys. Rev. B **42**, 2842 (1990).

[45] K. I. Bolotin, K. J. Sikes, Z. Jiang, M. Klima, G. Fudenberg, J. Hone, P. Kim, and H. L. Stormer, Ultrahigh electron mobility in suspended graphene, Solid State Commun. **146**, 351 (2008).

[46] N. García, P. Esquinazi, J. Barzola-Quiquia, B. Ming, and D. Spoddig, Transition from Ohmic to ballistic transport in oriented graphite: Measurements and numerical simulations, Phys. Rev. B **78**, 035413 (2008).

[47] Y. Wang, D. C. Alsmeyer, and R. L. McCreery, Raman spectroscopy of carbon materials: structural basis of observed spectra, Chem. Mater. **2**, 557 (1990).